

Investigating a shape memory epoxy resin and its application to engineering shape-morphing devices empowered through kinematic chains and compliant joints

Mana Nabavian Kalat^a, Maria Staszczak^a, Leszek Urbański^a, Carlos Polvorinos-Fernández^b, Carlos Aguilar Vega^b, Mariana Cristea^c, Daniela Ionita^c, Andrés Díaz Lantada^{b,*}, Elżbieta A. Pieczykńska^a

^a Institute of Fundamental Technological Research, Polish Academy of Sciences, Warsaw, Poland

^b Department of Mechanical Engineering, Universidad Politécnica de Madrid, Madrid, Spain

^c “Petru Poni” Institute of Macromolecular Chemistry, Iași, Romania

ARTICLE INFO

Keywords:

Shape memory polymers
Shape memory epoxy
Shape morphing structures
Laser stereolithography
3D and 4D printing

ABSTRACT

4D printing is the additive manufacturing (3D printing) of objects that can transform their shape in a controlled and predictable way when subjected to external stimuli. A thermo-responsive shape memory polymer (SMP) is a highly suitable material to 4D print smart devices, due to its actuation function and the capability of recovering its original shape from the deformed one upon heating. This study presents the results of employing an epoxy resin in the additive manufacturing of complex-shaped smart devices with shape-morphing properties using laser stereolithography (SLA). To quantify the shape memory behaviour of the shape memory epoxy (SMEp), we first investigate the thermomechanical properties of the 3D-printed specimens in a tensile testing machine coupled with an environmental thermal chamber. This approach allows us to determine the shape fixity and recovery of SMEp. Next, we propose effective designs of complex-shaped devices, with the aim of promoting shape morphing through micro-actuators and compliant joints acting as active regions in combination with multiplying mechanisms or kinematic chains in each of the devices. We manufacture the complex-shaped prototypes by using SLA directly from the computer-aided designs. The shape memory trials of the 3D-printed prototypes reveal quite precise shape recovery of the devices, illustrating their shape-memory. In fact, the inclusion of micro-actuators and compliant joints within the complex-geometry devices allows for local triggering, deformation and recovery, resulting in a prompt response of the devices to heat. Therefore, innovative designs, along with the suitable smart material and high-quality manufacturing process, lead to 4D printed devices with fast actuation and shape-morphing properties. Overall, this research may contribute to the development of smart materials and 4D printing technology for applications in fields such as biomedical engineering, robotics, transport and aerospace engineering.

1. Introduction

Shape-morphing structures are able to change their shape configuration in response to an external stimulus, in order to improve their interaction with the surrounding environment. A device with shape-morphing properties can undergo pre-programmed geometrical changes to perform a variety of actions, from very simple to highly specific tasks, linked to end applications. Due to their environmental sensitivity and adaptability, shape-morphing structures have already

made an impact in several industrial fields, from robotics to medicine, from architecture to inner design and from vehicles to aircraft and space technology. Deployable satellite structures, adaptive furniture, environmentally responsive façades, wind turbine blades, aircraft wings, minimally invasive surgical tools, tissue engineering scaffolds and adaptive implants benefit from implementation involving shape-morphing structures or shape-adaptive components manufactured with different families of shape-memory materials [1–4].

The applications of shape-morphing devices range from large-scale

* Corresponding author.

E-mail address: andres.diaz@upm.es (A. Díaz Lantada).

<https://doi.org/10.1016/j.matdes.2023.112263>

Received 27 June 2023; Received in revised form 8 August 2023; Accepted 19 August 2023

Available online 21 August 2023

0264-1275/© 2023 The Authors. Published by Elsevier Ltd. This is an open access article under the CC BY-NC-ND license (<http://creativecommons.org/licenses/by-nc-nd/4.0/>).

systems for buildings, vehicles, aircraft wings and machines, to micro/nano-manipulators, which are extensively manufactured for small-scale engineering applications such as micro-transporters [5], micro-grippers [6], micro-vascular [7] and micro-actuators [3,8]. An innovative approach to achieve precise manipulation of motions in a soft robot with complex geometry is to design and place a micro-actuator (typically a few centimetres) within the device. The actuator applies a force to change the configuration of the entire device in a pre-specified way once it is actuated by an environmental stimulus [9].

To obtain smart, complex-shaped devices with shape-morphing properties that can perform a pre-defined task in a specific environment, some essential factors must be considered: (a) choose a well-suited material for the shape-shifting purpose; (b) choose a proper stimulus to trigger the devices, depending on the application; (c) investigate and understand the mechanical behaviour and transformation ability of the material in response to the triggering stimulus; (d) design the devices according to their intended tasks to optimise their performance; and (e) choose a manufacturing process compatible with the selected material, design, shape, geometrical features and final application [10].

Among the most suitable candidate materials that can induce shape-shifting mechanism in engineering devices are stimulus-responsive materials with shape memory properties, namely shape memory alloys (SMAs) and shape memory polymers (SMPs). The former ones stand out for being high-performance actuators capable of exerting important forces during actuation, the latter outperform in the achievable deformations and lead to remarkable metamorphoses. Shape memory behaviour is the ability of a deformed shape memory material to recover its original or pre-determined shape after exposure to an external stimulus [11–13]. Heat is the most used external stimulus to activate and initialise the shape recovery process in a shape memory material. The glass transition temperature (T_g) and the melting temperature (T_m) of thermosensitive SMPs, used in a shape-morphing structure, are employed in many cases as the activation temperatures of the device [14].

The macroscopic shape memory behaviour of an SMP object in a thermomechanical cycle is presented schematically in Fig. 1. The

original state of the SMP before being activated and deformed is demonstrated in Fig. 1a. To investigate the shape memory behaviour, the object is first heated to above T_g , to reach the so-called rubbery phase of the polymer (Fig. 1b). The loaded SMP object of the next step (Fig. 1c) is subsequently fixed by being held and cooled down to below T_g to the glassy phase of the polymer (Fig. 1d), and then unloaded in a subsequent step (Fig. 1e). Afterwards, by increasing the temperature to above T_g , usually under zero stress, the original shape is almost completely recovered (Fig. 1f). In fact, the microscopic phase transition due to temperature variations above and below T_g activates the shape memory behaviour of the SMP by storing and releasing the elastic energy in the cooling and heating steps, respectively [14,15]. This conventional framework of thermomechanical programming in a coupled system of a mechanical loading testing machine and an environmental thermal chamber leads to the determination of two shape memory parameters of the SMP: shape fixity and recovery [16]. Determination of shape fixity of a SMP enables one to quantify approximately the temporary deformation that the material can retain when the temperature is lower than T_g , while determination of shape recovery reveals the deformation that the material can recover at a temperature above T_g . Estimation of the shape memory parameters through a thermomechanical cycle leads to choose suitable applications in which the SMP could function effectively without in-service failure.

SMPs have shown great potential in the field of robotics [17] due to their unique shape recovery behaviour upon being heated. Employing SMPs in robotics enables the development of lightweight, quite flexible and responsive robots that can mimic biological movements and adapt to their environment. However, optimising the material properties as well as designing and developing a reliable manufacturing process to obtain complex-shaped devices is still challenging.

Indeed, designing a device with complex geometry containing a micro-actuator that could perform a pre-specified shape-shifting task requires a deep understanding of the actuation mechanisms. To ensure the devices function as intended and perform the desired motions with accuracy and efficiency, it is necessary to find an optimal location for the actuators. In addition, the actuators' sizes and shapes must fit within the

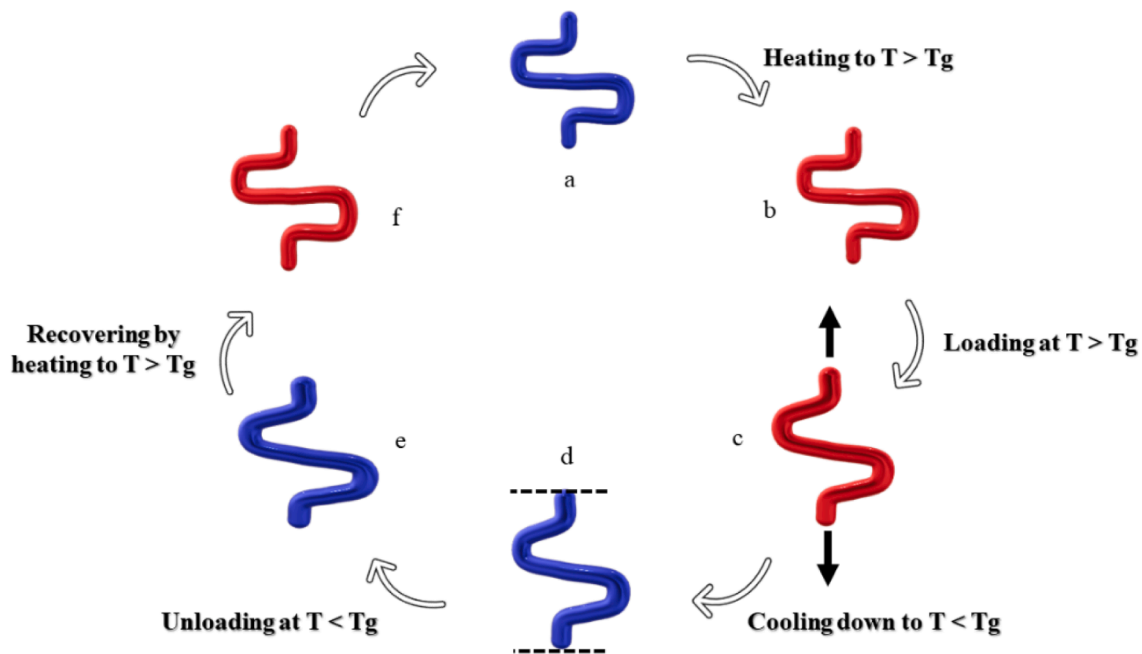


Fig. 1. Schematic drawing of shape memory behaviour of an SMP object in a thermomechanical cycle: (a) original state of the SMP; (b) SMP heated to temperature $T > T_g$; (c) SMP loaded at $T > T_g$; (d) SMP cooled down to $T < T_g$ while keeping the strain; (e) SMP unloaded at $T < T_g$; (f) the thermally recovered SMP after being heated to $T > T_g$.

device constraints.

Fabrication of polymeric complex-shaped objects by traditional techniques, as well as time-consuming post-processes and assembly operations, can become less challenging by employing additive manufacturing (AM) technologies, popularly referred to as 3D printing. AM technologies, usually following a layer-by-layer approach, enable the creation of detailed objects with complex geometries directly from a computer-aided design file in a single step. 3D printing of stimulus-responsive devices from smart shape memory materials [18,19] has recently been integrated under the term 4D printing [20–22]. 4D printing results in the fabrication of dynamic and adaptive parts, unlike the inactive objects obtained by 3D printing. However, in terms of precision and achievable complexity, additive photopolymerisation approaches – for example, the laser stereolithography (SLA) 3D printing method – still seem to be the best options to construct complex shape-morphing objects with high printing resolution and manufacturing precision. In the SLA 3D printing method, the free surface of the photosensitive resin liquid is polymerised selectively, layer-by-layer, with laser beam radiation with a power and frequency suited to the type of resin. By selecting a suitable material, this process can produce polymerised solid prototypes with shape memory properties [23–25].

Previous studies have proposed straightforward development methods for smart devices based on SMPs, processed additively by SLA as a key enabling technology [26]. Despite these developments, there is still a need for systematic studies that characterise the thermomechanical properties of processed thermoresponsive polymers, as well as design, 4D printing and training for final applications. Indeed, the quantified shape memory behaviour of a smart polymer enables the user to predict the material's final performance.

Given the aforementioned need, this study focuses on the thermo-mechanical characterisation of an industrial gold standard epoxy resin (called SMEp in this study), which is additively manufactured by using the SLA 3D printing technology. To the best of our knowledge, the shape memory parameters of this type of epoxy, suitable for high-resolution 4D printing of smart complex devices, have not yet been investigated. The obtained results helped us with the design and training of high-performance smart devices that we additively manufactured from SMPs.

The first part of this study provides a quantitative understanding of the behaviour of the chosen SMEp. We determined T_g of the cross-linked SMEp through thermogravimetric analysis (TGA) and differential scanning calorimetry (DSC), and then performed mechanical characterisation of the material at two different temperatures (20 °C below and 20 °C above T_g). To investigate the material properties, we carried out a thermomechanical cycle on 3D-printed SMEp specimens, allowing us to quantify the shape memory parameters. In the second part of the study, we propose innovative designs for smart complex-shaped devices containing micro-actuators and a compliant joint.

Prototypes are manufactured directly from computer-aided designs by using the SLA 3D printing method in a single step. The whole devices are printed by employing SMEp, but the designs have specific active regions, namely the micro-actuators or the compliant joint. Therefore, by heating and deforming the devices from the active region, rest of the structure remains almost undeformed and global shape-morphing is achieved by amplifying geometrical mechanisms and kinematic chains. After manufacturing, the shape memory prototypes were subjected to a shape memory cycle, including training and recovery, based on the findings of the thermomechanical investigation to confirm shape-morphing behaviour of the complex geometries. Finally, the limitations of the study, future research directions, and potentials for 4D printed SMEp-based devices are presented and discussed.

2. Materials and methods

2.1. Materials

A multipurpose and widely available epoxy resin for laser

stereolithography should be selected for making our study replicable and useful for the community of users of laser stereolithography systems. Other thermosets usable in laser stereolithography and UV photopolymerization systems including digital light processing low-cost printers could have been selected, and similar characterization processes and design methods applied.

In this study, we opt for epoxy resin SOMOS WaterShed R XC11122 (DSM Desotech BV, Slachthuisweg 30, 3151 XN Hoek van Holland, the Netherlands), which is a photopolymerisable prototyping material that is suitable for AM of highly detailed parts with high resolution, toughness and water resistance, according to the material's data sheet and standardized tests. These parts can mimic the look and performance of thermoplastic polymers such as acrylonitrile butadiene styrene (ABS) and polybutylene terephthalate (PBT). Besides, the resin is compatible with laser stereolithography systems from the two main developers of this technology (3D Systems and Stratasys).

2.2. Methods

2.2.1. Thermal characterisation

TGA and DSC experiments were conducted on the cross-linked sample to determine the thermal stability and to verify the T_g of the post-cured epoxy. Thermogravimetric analysis of the crosslinked SMEp sample was performed on a Discovery TGA 5500 (TA Instruments, USA), at a heating rate of 10 °C/min. The sample with a weight of 6.2 mg was placed in a platinum crucible and was heated from room temperature up to 700 °C under a flow of N₂ (25 mL/min).

DSC analyze was carried out by a Discovery DSC 250 (TA Instruments, USA), also under an N₂ atmosphere. The specimen with a weight of about 6.4 mg was sealed in aluminum crucibles. A heating/cooling/heating program with a 10 °C/min heating rate was employed in the temperature range between 0 °C and 200 °C. T_g of the cross-linked SMEp was determined from the inflection point of the heat flow curve of the second heating.

2.2.2. Mechanical and thermomechanical characterisation of SMEp

2.2.2.1. Specimen. The shape and dimensions of the dog-bone specimens (Fig. 2a, b) for uniaxial tensile loading in mechanical and thermomechanical investigation were selected on the basis of many preliminary studies conducted by the authors on this type of material. One of the objectives was that the specimen cracked in the centre when it was loaded until break. Such specimens were printed with laser SLA. This 3D printing process involves selective layer-by-layer polymerisation of a photosensitive epoxy resin liquid, using laser beam radiation, with an appropriate power and frequency for the specific type of resin. The orientation of the printed layers with respect to the build platform leads to an anisotropic structure with anisotropic thermal and mechanical properties.

To avoid the effect of printing orientation on the mechanical and shape memory behaviour of the specimens and obtain repeatable results, all specimens were printed layer-by-layer from the lateral edge of the dog-bone geometry. Therefore, the uniaxial elongation of the specimens during mechanical investigation was carried out in line with the printing orientation (x direction) (Fig. 2b). The final 3D printed specimen is demonstrated in Fig. 2c.

2.2.2.2. Experimental methods and conditions. The mechanical and thermomechanical behaviours of SMEp were investigated using a tensile testing machine (Instron 5969), coupled with the Instron environmental thermal chamber to control the temperature (Fig. 2d), under the tension mode at the strain rate of 10⁻² s⁻¹. Investigation of the mechanical features of SMEp in a tension loading to rupture at $T_g - 20$ °C = 25 °C (room temperature) and $T_g + 20$ °C = 75 °C helps to choose an appropriate deformation range for the thermomechanical programming.

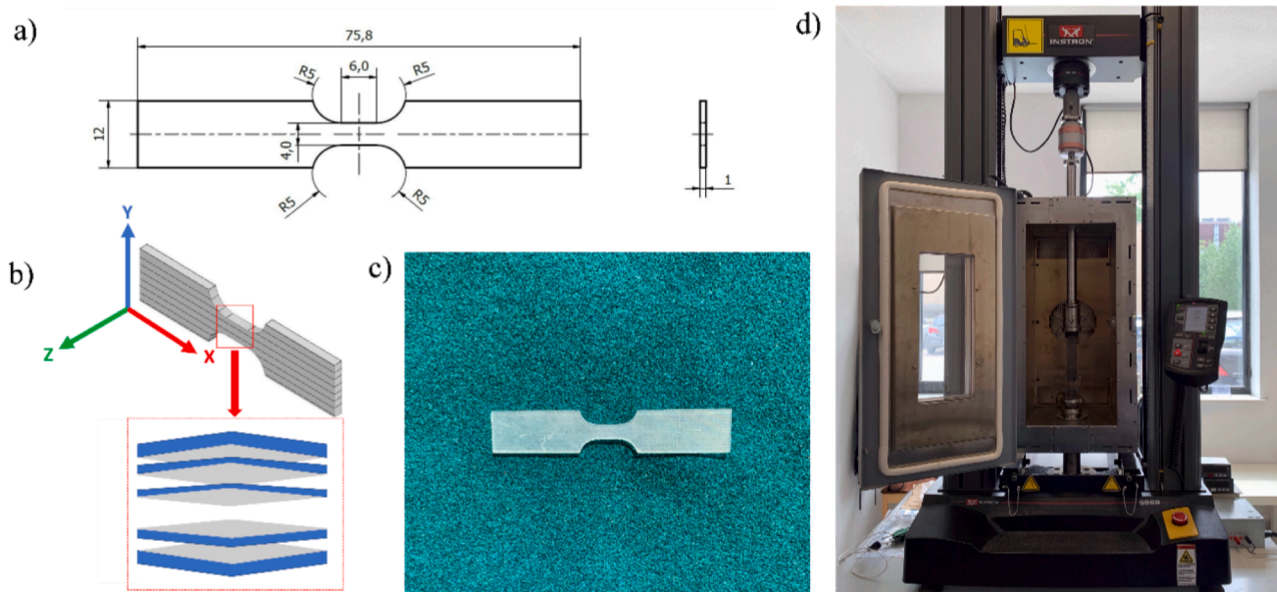


Fig. 2. (a) Dimensions of the dog-bone-shaped SMEp specimen, which is standard for mechanical and thermomechanical investigations. (b) Schematic of the dog-bone-shaped specimen printed layer-by-layer from the lateral edge with SLA 3D printing. (c) A picture of a 3D-printed SMEp specimen. (d) Coupled system of a tensile testing machine inside an environmental thermal chamber.

The shape memory behaviour of the SMEp was examined within a thermomechanical loading program conducted inside the thermal chamber. In the first step of the thermomechanical cycle, the SMEp specimen was placed in the grips of the tensile machine and heated to $T_g + 20$ °C with heating rate of 12 °C/min) under zero force. The thermal elongation of the specimen under the no-load conditions was recorded by the testing machine. In the second step, the heated specimen was uniaxially loaded with the strain rate of 10^{-2} s $^{-1}$ to a specific strain, determined based on the elongation at break value obtained from the initial mechanical investigation. Subsequently, the deformed specimen was cooled to $T_g - 20$ °C (room temperature), while maintaining the obtained maximum strain value. Next, the cooled specimen was unloaded with the strain rate of 10^{-2} s $^{-1}$ to the zero force, to fix the temporary shape at $T_g - 20$ °C. Eventually, the specimen was again heated to $T_g + 20$ °C with heating rate 12 °C/min under zero force, in order to estimate the shape recovery of the SMEp.

Due to the significant value of thermal elongation observed in the first step of heating, the ability of SMEp to fix and recover thermal elongation during heating was investigated separately in a recommended framework of the thermomechanical cycle without mechanical loading. In this framework, the SMEp specimen was heated to $T_g + 20$ °C with the rate 12 °C/min) under no tensile load while placed between the grips inside the thermal chamber. The thermal elongation of the specimen was recorded. Thereafter, the thermally elongated specimen in the tensile grips was cooled to $T_g - 20$ °C with the rate 12 °C/min. The contraction stress resulting from cooling the specimen, which was unloaded with the strain rate of 10^{-2} s $^{-1}$ to zero force in the next step and has the temporary thermally deformed shape, was obtained. Finally, the specimen was heated to $T_g + 20$ °C at 12 °C/min under no load inside the thermal chamber to recover the initial shape.

2.2.3. Design, manufacturing and training of the SMEp prototypes

2.2.3.1. Designs. SLA can be used to 3D print detailed and complex physical parts directly from computer-aided designs. The great advantages of this technology are the promotion of personalised production, the integration of functionalities through geometrical complexity and the possibility of processing shape memory polymers into stimulus-responsive, high-resolution and high-quality devices. SLA was the first

AM technology that has developed and achieved a substantial industrial impact. It still provides remarkable results with an acceptable compromise between achievable size, surface roughness, aesthetic aspects and mechanical performance.

For this study, the complex-shaped prototypes of different mechanisms and smart structures, actuated with a driving shape-morphing element, were designed with NX-12 (Siemens PLM Solutions, Germany), in an attempt to obtain the benefit of the singular features of SLA. Proof-of-concept structures, amplifying kinematic chains (mechanical mechanisms) and compliant joints were designed to validate the utility of shape morphing in conceptual devices and to illustrate the empowering ability of the mentioned kinematic chains and compliant joints.

Computer-aided designs of the devices are presented in Fig. 3a. The overall thickness of all devices, including the truss cross-sections of the mechanisms and the structures, is 800 μ m, while the thickness of the S-shaped actuators and torsional springs is 350 μ m. Therefore, the structural elements are quite thicker than the S-shaped and torsional springs to promote the localised action.

2.2.3.2. Prototypes. Once designed, the prototypes were submitted to AM using an SLA-3500 laser SLA machine developed and commercialised by 3D Systems (Rock Hill, SC, USA). The designs of the shape-morphing devices prepared for slicing and printing with SLA are presented in Fig. 3b, with the SLA printing platform shown at the bottom. Structures are shown in purple, while supports to enable the SLA construction are highlighted in pale orange.

After slicing with the support of 3D Lightyear software (3D Systems), a companion to the SLA system, the laser beam trajectories that polymerise the resin were defined. The laser activates a polymerisation reaction layer-by-layer to generate complex 3D structures. A final post-curing step in an ultraviolet (UV) oven for 10 min, according to the photoresin's specifications and considering the small size of manufactured parts, leads to the desired master structures.

The final printed prototypes containing an S-shaped actuator, in the form of a shape-memory spring, are shown in Fig. 3c, as the first three devices from the left. All kinematic chains are governed by the same spring-shaped actuator (circled in red), which connects all parts in their central region and acts as an active region. Although the entire structure is printed using SMEp, the thinner cross-section of the S-shaped micro-

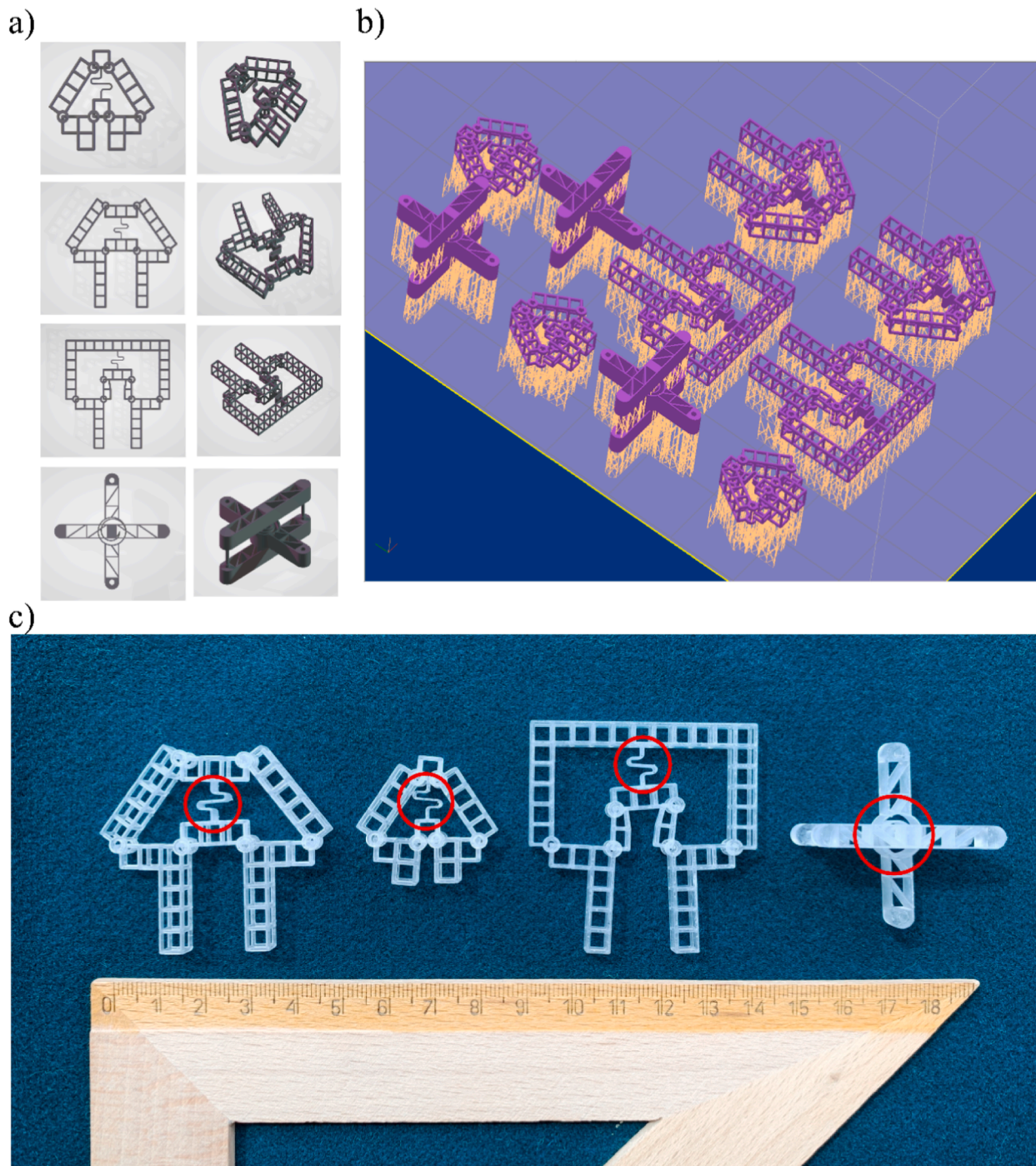


Fig. 3. (a) Computer-aided designs of the devices. (b) Designs of shape-morphing devices for slicing and 3D printing by SLA. Structures are shown in purple, while supports that enable the SLA construction are highlighted in pale orange. (c) The final 3D-printed SMEp prototypes. The first three prototypes contain an S-shaped actuator (circled in red) to control the configuration changes and a compliant torsional spring in the t-shaped device to change the angle between the arms.

spring makes it the actual active region, which is deformed during the shape-memory training process. The mechanisms of movements in the devices are blocked in the rigid state of the S-shaped micro-spring, while during the shape memory trial, these over-constrained mechanisms acquire one degree of freedom, and the linear deformation of the actuator moves the entire structure in a predefined way. In addition, another design based on a compliant joint with a central active region is shown as the last device from the left in Fig. 3c. The compliant torsional spring in this t-shaped device acts as an active region, located at the connection point of the perpendicular arms. The spring is thinner than other regions

of the structure, which simplifies its deformation during shape-memory training, as in the previous case.

2.2.3.3. The shape memory trial. The steps of the shape memory cycle were carried out, as in the thermomechanical investigation, to train the shape memory effect of the 3D-printed devices. Due to the moisture-resistance of the SOMOS Watershed XC 11122, the printed SMEp prototypes can be activated and reach the triggering temperature above T_g by direct contact with hot water, which shortens the response of the device due to the higher convection coefficient of water compared with

heating in air. The presence of the actuator in each device as a connecting element allows conducting the training cycle just on the actuator, while simultaneously the configuration of the whole device changes in a desired way, through the action of kinematic chains or compliant joints. Therefore, the S-shaped or torsional actuator in each device was locally heated by hot water at around $75\text{ }^{\circ}\text{C}$ ($T_g + 20\text{ }^{\circ}\text{C}$). The hot water was applied with a syringe to just the actuator, to minimise the area that was heated. The deformation mechanism of the entire device occurred by stretching the heated actuator or by changing the intersection angle in the t-shaped device. The deformed actuator was locally cooled with cold water at approximately $25\text{ }^{\circ}\text{C}$ ($T_g - 20\text{ }^{\circ}\text{C}$), while keeping the deformation. After removing the force and obtaining the temporarily deformed device, the recovery trial was carried out by locally heating the actuator with hot water at around $75\text{ }^{\circ}\text{C}$ ($T_g + 20\text{ }^{\circ}\text{C}$). The apex angles in the joint parts of the devices or in the intersection of the t-shaped device, presented in Fig. 3c, were measured after the deformation and after the thermal recovery of the actuator with ImageJ software, to obtain an approximate value of the shape recovery of the entire geometry when just the actuator was triggered.

The FLIR A655sc thermal imaging camera (Sweden) was used to

detect the temperature profile in the prototypes during the actuation. Each device was placed at the optimised distance from the camera, and the camera was set to measure temperature in a specific range. The FLIR software was used to analyse the images captured and to calculate the temperature distribution of the material. The measurements were repeated several times to check the accuracy and to ensure the reproducibility of the results.

3. Results and discussion

3.1. Thermal and mechanical characterisation of SMEp

Thermal characterisation of cross-linked SMEp with TGA (Fig. 4a) and DSC (Fig. 4b) was carried out to determine thermal stability and the range of activation temperatures after cross-linking the epoxy resin. As shown in Fig. 4a, the weight percentage versus temperature curve (blue line) indicates that SMEp begins losing 5% of its weight at around $292\text{ }^{\circ}\text{C}$. The peak value in the weight derivative curve (red line) in Fig. 4a corresponds to the degradation temperature of SMEp at the maximum decomposition rate, showing major weight loss; it is

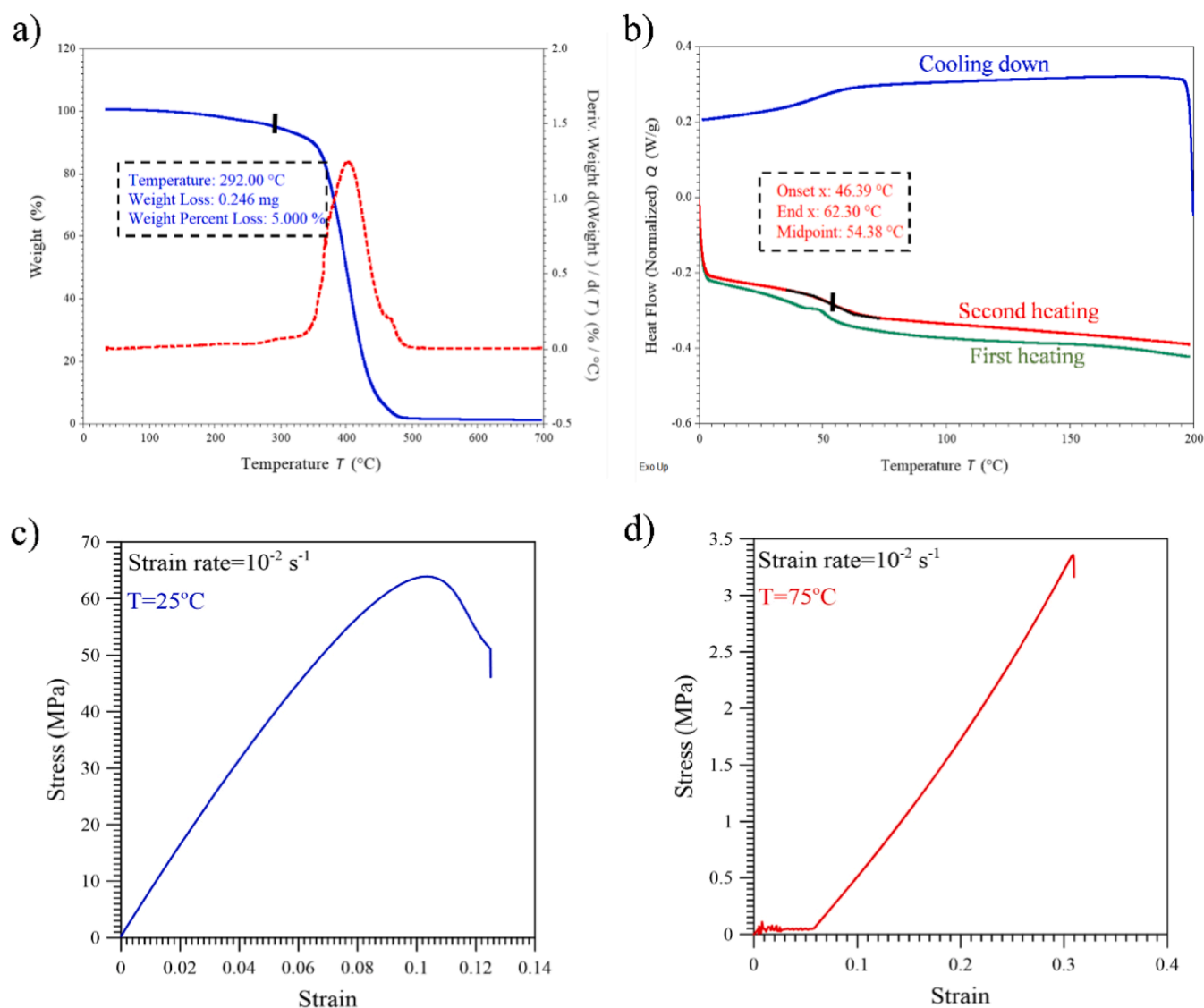


Fig. 4. (a) TGA results of cross-linked SMEp, indicating its thermal stability. (b) DSC results of cross-linked SMEp, indicating the activation temperature. (c) The stress-strain curve of the SMEp specimen subjected to uniaxial tensile loading until rupture at ambient temperature. (d) The stress-strain curve of the SMEp specimen subjected to uniaxial tensile loading until rupture at $75\text{ }^{\circ}\text{C}$ ($T_g + 20$).

approximately 400 °C.

T_g of a SMP determines the activation temperature of the polymer segments at which the material can be deformed or recovered. Therefore, T_g is a crucial factor in deciding the application of a thermosensitive SMP. We performed DSC by investigating heat flow versus temperature to determine T_g of SMEp. The start and end points of the step appearing in the second heating of DSC (red line) in Fig. 4b are considered to be the range of activation temperature of the material; these temperatures are 46 and 62 °C. T_g is considered to be the midpoint of the step's tangent, which is about 54 °C, indicating the temperature above which the SMEp device can be deformed and recovered and below which the deformed device can be fixed.

Investigating the mechanical sensitivity of an SMP to heat is crucial to assess its potential application in thermally actuated devices. Moreover, understanding the dependence of elastic and plastic behaviours of an SMP on temperature is important to select an appropriate deformation range later in the thermomechanical investigation while considering the material's strength and deformation tolerance. To investigate the mechanical behaviour of 3D printed dog-bone shaped SMEp specimens, we obtained typical stress–strain curves by subjecting the samples to uniaxial tensile loading with a constant strain rate of 10^{-2} s^{-1} until rupture. The results of the tests conducted at room temperature (below T_g) and at 75 °C ($T_g + 20$ °C) are shown in Fig. 4c and Fig. 4d, respectively. We carried out the experiments in an environmental chamber to ensure that the SMEp specimens were exposed to a controlled temperature.

To ensure repeatability, we performed the mechanical tests on three 3D-printed SMEp specimens at each temperature. They exhibited nearly identical behaviour and the stress–strain curves in Fig. 4c and Fig. 4d represent the mean values. Accordingly, the mean values of mechanical properties, including Young's modulus, ultimate strength and elongation at break, below and above T_g , are presented in Table 1. Young's modulus drops as the temperature increases during loading due to the mobility of the polymer chains at high temperature. Similarly, the ultimate strength of the polymer, which is the maximum stress before the material failure, decreases for the same reason. Consequently, the elongation at break increases as the testing temperature rises because of the flexibility of the polymer at temperatures above T_g [14].

According to the tensile stress–strain curve of the SMEp specimen at ambient temperature (Fig. 4c), due to its brittle nature, the material fails right after high yield stress and before any necking or strain hardening. This phenomenon indicates that the material is not suitable for plastic deformation at room temperature, so-called cold programming [27,28].

However, at a high temperature, the thermoset SMEp elongates to the higher strains and fails without showing any sharp yield point in the stress–strain curve (Fig. 4d). Therefore, to achieve the elastic–plastic behaviour in this SMP, hot-programming is crucial in the thermo-mechanical loading cycle.

On the other hand, heating a smart SMP device for actuation may present challenges. In fact, low thermal conductivity of polymers leads to a time-consuming heating process and an undesirable thermal gradient within the device [7]. Additionally, the phase transition in the conventional process of the thermomechanical cycle (heating, loading, cooling down, unloading and heating) causes inevitable volume changes in the polymer. As shown in Fig. 5b, the material displays about 6% thermal elongation under almost zero stress, reaching and stabilising at

75 °C in the thermal chamber before loading. The thermal gradient and thermal expansion during heating limit the application fields of the smart polymer, in which fast actuation, dimensional stability and a low thermal expansion coefficient are important for applications in electronic components or aerospace structures.

3.2. Thermomechanical characterisation of the 3D-printed SMEp specimens: Estimation of shape fixity and shape recovery

To quantify the shape memory properties and to determine the shape fixity and shape recovery values of the printed SMEp dog-bone specimen, we conducted a thermomechanical cycle. We used a tensile testing machine coupled with an environmental thermal chamber. To ensure the repeatability of the results, we performed the cycle on four similar SMEp specimens. The stress–strain behaviour of one of the specimens is shown in Fig. 5a.

The thermomechanical cycle consists of the following steps:

1. Heat the specimen, held between the tensile grips in a thermal chamber, to 75 °C ($T_g + 20$ °C), with no applied force (red line Fig. 5a). When the thermal chamber temperature reaches 75 °C, continue for 1 min to reach a stable temperature.
2. Tension load the specimen by the strain value of 0.18 at a constant strain rate of 10^{-2} s^{-1} (purple line Fig. 5a). We chose the strain range for the tension loading based on the mechanical behaviour of SMEp at 75 °C ($T_g + 20$ °C), discussed in the previous section (Fig. 4d), to avoid rupture during loading.
3. Cool the specimen to room temperature while maintaining the maximum strain (blue line Fig. 5a).
4. Unload the specimen to almost zero force at a constant strain rate of 10^{-2} s^{-1} (green line Fig. 5a)
5. Heat the specimen in a thermal chamber to 75 °C ($T_g + 20$ °C), under zero force, to enable recovery of its original shape (black line Fig. 5a).

As mentioned previously, a changing issue encountered in the hot programming of polymers is thermal elongation, which acts against the shape recovery process [29]. As shown in the first step of the cycle (red line in Fig. 5a), the thermoset SMEp specimens with a brittle nature experience uniaxial thermal elongation before any loading during the heating process to reach 75 °C ($T_g + 20$ °C) from room temperature. The inevitable thermal elongation leads to the deformation of the material beyond the pre-programmed value. Moreover, Sedat et al. [29] found that thermal expansion may prevent shrinkage during the shape recovery process of deformed SMP; therefore, the material performance is limited. In this study, to determine shape fixity and recovery of SMEp more accurately compared with previous studies, we considered both uniaxial thermal elongation during the first step of heating and mechanical elongation during the second step as relevant aspects of global deformation. This approach enabled us to assess whether SMEp is capable of fixing and recovering the deformation resulting from both thermal and mechanical elongation, as both of these factors contribute to the global deformation of the material.

We determined shape fixity S_f and shape recovery S_r from the obtained experimental results (Fig. 5a) by using Eqs. (1) and (2), respectively, proposed by Tobushi and Hayashi [16].

$$S_f = \frac{\varepsilon_{un}}{\varepsilon_m} \bullet 100\% \quad (1)$$

$$S_r = \frac{\varepsilon_m - \varepsilon_{ir}}{\varepsilon_m} \bullet 100\% \quad (2)$$

In these equations, ε_m is the maximum strain after loading the specimen at 75 °C ($T_g + 20$ °C), ε_{un} is the strain obtained after unloading at room temperature (below T_g) and ε_{ir} is the irrecoverable strain after heating up to 75 °C ($T_g + 20$ °C) under zero force.

Table 1

The mean values of mechanical properties at 25 °C ($T_g - 20$ °C) and at 75 °C ($T_g + 20$ °C).

Mechanical properties	Values at $T_g - 20$ °C = 25 °C	Values at $T_g + 20$ °C = 75 °C
Young's modulus (MPa)	806.6105	10.89
Ultimate strength (MPa)	63.9341	3.63
Elongation at break (%)	13.05	32.00

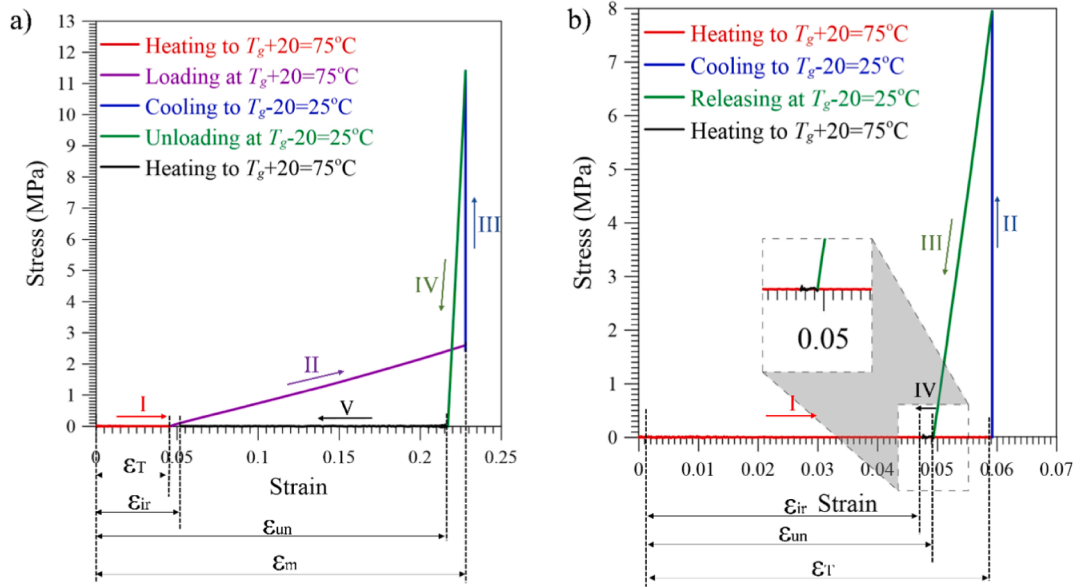


Fig. 5. The stress–strain curve obtained (a) from the thermomechanical loading cycle conducted on an SMEp specimen and (b) from the thermomechanical cycle conducted on an SMEp specimen deformed by thermal expansion, without any loading. The colours indicate subsequent stages of the cycle.

Table 2 shows the shape fixity and recovery values calculated for four similarly printed SMEp specimens as well as the averages of these two parameters. Moreover, the determined thermal elongation (ϵ_T) quantities resulting from the first step of heating in each specimen are shown. The thermal elongation before any loading results in the deviation of the deformation (ϵ_m) from the pre-specified value. Based on these results, greater thermal elongation leads to less shape recovery. As a result, the significant value of irrecoverable strain (ϵ_{ir}) and the difference in shape recovery values among similarly printed specimens may be due to the negative effect of thermal elongation upon strain recovery. However, it is worth noting that the shape fixity values are high and almost identical across all printed specimens.

To prove the negative impact of thermal elongation on the shape memory behaviour of the printed SMEp specimens, we evaluated the shape fixity and recovery parameters in a recommended framework of the thermomechanical cycle in which the specimen is elongated only due to heating, without any loading. Accordingly, we heated the specimen, which is positioned between the grips of the tensile testing machine, in an environmental thermal chamber from room temperature to 75 °C ($T_g + 20$ °C) at zero force (red line in Fig. 5b) and kept it for 1 min to reach a stable temperature. We then cooled the thermally elongated specimen from 75 °C ($T_g + 20$ °C) to room temperature by keeping the thermal elongation constant, leading to increase in stress recorded by the tensile grips (blue line in Fig. 5b), due to contraction of the specimen during the cooling down step. We subsequently released the contraction stress to zero stress (green line in Fig. 5b). To calculate the strain recovery, we reheated the thermally deformed specimen to 75 °C ($T_g + 20$ °C) while still keeping it in the tensile grips (black line in Fig. 5b).

We calculated the shape fixity S_{fT} and shape recovery S_{rT} of the thermally deformed specimen by modifying equations (1) and (2) to Eq. (3) and Eq. (4), respectively.

The results are shown in Table 3

Table 2

Shape memory parameters and thermal elongation (in the process of reaching 75 °C from room temperature) of four SMEp specimens.

	First specimen	Second specimen	Third specimen	Fourth specimen	Average
ϵ_T (%)	6.86	4.639	4.610	3.697	4.949 ± 1.20
S_f (%)	95.21	95.07	95.38	94.52	95.045 ± 0.33
S_r (%)	64.50	77.01	77.05	80.65	74.80 ± 8.21

Table 3

Shape memory parameters and thermal elongation (in the process of reaching 75 °C from room temperature) of the SMEp specimen elongated due to only thermal expansion.

ϵ_T (%)	5.92
S_{fT} (%)	83.33
S_{rT} (%)	19.72

$$S_{fT} = \frac{\epsilon_{un}}{\epsilon_T} \cdot 100\% \quad (3)$$

$$S_{rT} = \frac{\epsilon_T - \epsilon_{ir}}{\epsilon_T} \cdot 100\% \quad (4)$$

In Eqs. (3) and (4), ϵ_T is thermal elongation strain due to heating of the specimen from room temperature to 75 °C ($T_g + 20$ °C) under the no-load condition, ϵ_{un} is the strain obtained after unloading the contraction stress at room temperature (below T_g) and ϵ_{ir} is the irrecoverable strain after heating up to 75 °C ($T_g + 20$ °C) under the no-load condition.

The shape fixity and recovery values in Table 3 suggest that SMEp is almost incapable of restoring its original shape after undergoing thermal elongation, either by unloading at room temperature or by heating. Generally, heating a polymer increases chain mobility and the molecular entropy state. Due to temperature gradients in polymers, it is sometimes necessary to maintain the polymer at a high temperature for an extended period of time to achieve the desired temperature. This extended heating allows for a relaxation process to take place within the material. According to Lendlein et al. [30], relaxation leads to irreversible deformation. Therefore, thermal deformation is irreversible and leads to high irrecoverable strain values in shape memory polymers. Hence,

applications using methods or designs to decrease the heating time is of importance to achieve fast actuation without a temperature gradient and thermal expansion within the shape-morphing devices.

3.3. Shape memory effect activation trials in the 4D-printed prototypes

Thermoresponsive SMPs offer great potential to 4D print complex smart devices with shape-morphing properties, because their phase transformations (by changing temperature in a thermomechanical cycle) allow them to fix and recover deformation and activate the shape-shifting property of the smart device. We printed high-resolution, high-quality complex-shaped SMEp smart prototypes directly from computer-aided designs in a single step, by using laser SLA via additive photopolymerisation of the epoxy resin.

Within the complex-shaped SMEp prototypes presented in Fig. 6, an active region is incorporated as a S-shaped actuator. It serves to interconnect all components of the device and to prevent unexpected movements. The actuator is intentionally designed and printed to be thinner than the other regions in each device, facilitating its deformation and promoting its localised action while other parts of the device are not deformed. The actuator acts as a multiplying element due to its purposely designed kinematic chains, mechanisms or compliant regions, as described previously. Fig. 6 shows the importance of the actuator within the complex geometry. In the top row, the S-shaped actuators connect the two parts of each device, resulting in constraining the entire device. In contrast, in the bottom row the device movement is not constrained because there is no actuator.

In each prototype, a pre-specified shape-shifting task can be performed by heating, deforming, cooling and thermal recovery of the connecting shape-morphing actuator. Conducting the shape memory trial just on the actuator eliminates the need to heat and deform the entire device, resulting in a shorter actuating time, reduced temperature gradients across different parts and less thermal expansion in the devices. In addition, because the material is water resistant, these devices can be used in water, meaning that the actuator can be heated and cooled by hot and cold water.

Here, we investigated the effect of the shape memory behaviour of SMEp on the mechanism of motion in the printed prototypes within a thermomechanical cycle. We designed the prototypes, containing S-shaped actuators, to open through hot deformation, to stay fixed when cooled and then to close again through thermal recovery. The t-shaped device, with the compliant torsional spring, alters its configuration by changing and recovering the angle at the intersection of the arms. As

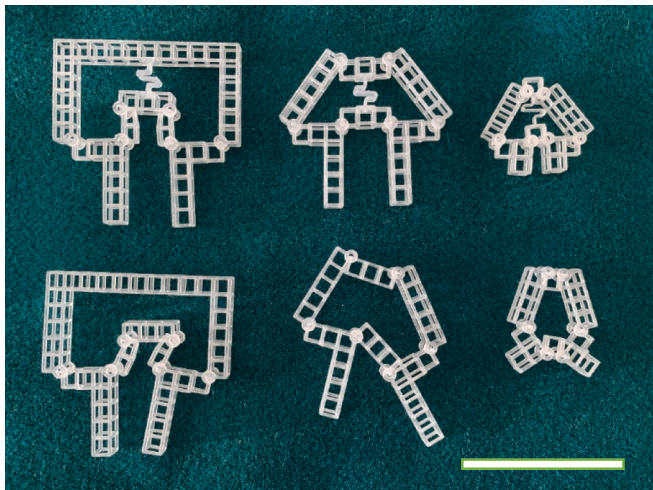


Fig. 6. The top row shows 3D-printed SMEp prototypes containing actuators (over-constrained in the rigid state of the actuator). The bottom row shows 3D-printed prototypes without actuators (under-constrained). Bar: 40 mm.

noted previously, only the actuator part of the device, rather than the entire device, is subjected to the shape memory cycle.

Fig. 7a shows the original state of one of the 3D-printed prototypes, with the S-shaped active region. We started the shape memory trial of the device by locally heating the actuator with hot water at approximately 75 °C ($T_g + 20$ °C) (Fig. 7b). The other regions of the device remain unheated. Subsequently, the whole device is deformed just by stretching the heated actuator (Fig. 7c). We cooled just the deformed actuator with cold water at approximately 25 °C ($T_g - 20$ °C) while keeping the deformation constant. We then removed the force to obtain the temporarily deformed device (Fig. 7d). By locally heating the deformed actuator with hot water under no force ($T_g + 20$ °C = 75 °C) (Fig. 7e), we recovered the original shape of the actuator and, consequently, the entire device (Fig. 7f). The t-shaped device undergoes the same steps of the thermomechanical cycle, by local heating of the torsional spring using hot water (75 °C), changing the angles between the arms manually from 90° to almost 10° (not zero due to design limits), fixing the angle by local cooling of the torsional spring using cold water (25 °C) and restoring the original shape by local heating of the actuator by hot water (75 °C).

Supplementary Materials S1_X_Y includes videos of the thermomechanical trial of each device, being X the device number according to Table 4, and with Y taking the values: 1, for the training process, or 2, for the shape-memory recovery.

In fact, in each device, the recovery of the deformed actuator in response to hot water applies force to all parts of the prototype and leads to recovery of the entire prototype. During thermomechanical training, the actuator responds to hot or cold water – triggering, fixation or recovery – within a maximum of 10 s, without the need to heat or cool down the entire device. Therefore, the design of these kinds of devices, containing an actuator or active region that amplifies movement through kinematic chains or mechanisms, along with a suitable smart material and high-quality manufacturing process, lead to fast actuation and remarkable shape morphing.

Fig. 8 illustrates the temperature profiles of one of the 3D-printed prototypes with the S-shaped actuator during various stages of the thermomechanical cycle. This figure highlights the potential to change the configuration of the entire device in different steps, by performing the thermomechanical programming on just the connecting actuator, while the temperature of the other parts remains almost unchanged.

Fig. 9a, b and c show the original, deformed and recovered shape of the 3D-printed complex-shaped prototypes, respectively, programmed in a thermomechanical trial showed in Fig. 7. The average left and right apex angles before and after shape recovery in the first three types of devices (shown in red) can serve as suitable parameters to estimate the approximate values of deformation and shape recovery in the 3D-printed SMEp prototypes. These values can be estimated by determining the intersection angle in the t-shaped device (shown in red).

To ensure accuracy, we measured the angles in each device multiple times using ImageJ software on two separate devices of each type. All three types of prototypes exhibit minimal changes in apex angles after cooling the deformation and unloading (Fig. 7, step c to d). Therefore, we assume that the shape fixity of the prototypes is almost 100%, indicating a high level of shape retention, even after removing external forces. Thus, we only estimated the shape recovery of the devices. We calculated the approximate values of shape deformation and recovery in each prototype by using Eqs. (5) and (6).

$$S_d = \frac{\theta_m - \theta_0}{\theta_0} \cdot 100\% \quad (5)$$

$$S_{r,\theta} = \frac{\theta_m - \theta_{ir}}{\theta_m} \cdot 100\% \quad (6)$$

In Eqs. (5) and (6), θ_0 is the initial value of the angle (Fig. 9a), θ_m is the angle in each device after deforming at 75 °C ($T_g + 20$ °C) and cooling to 25 °C ($T_g - 20$) (Fig. 9b) and θ_{ir} is the irrecoverable angle after

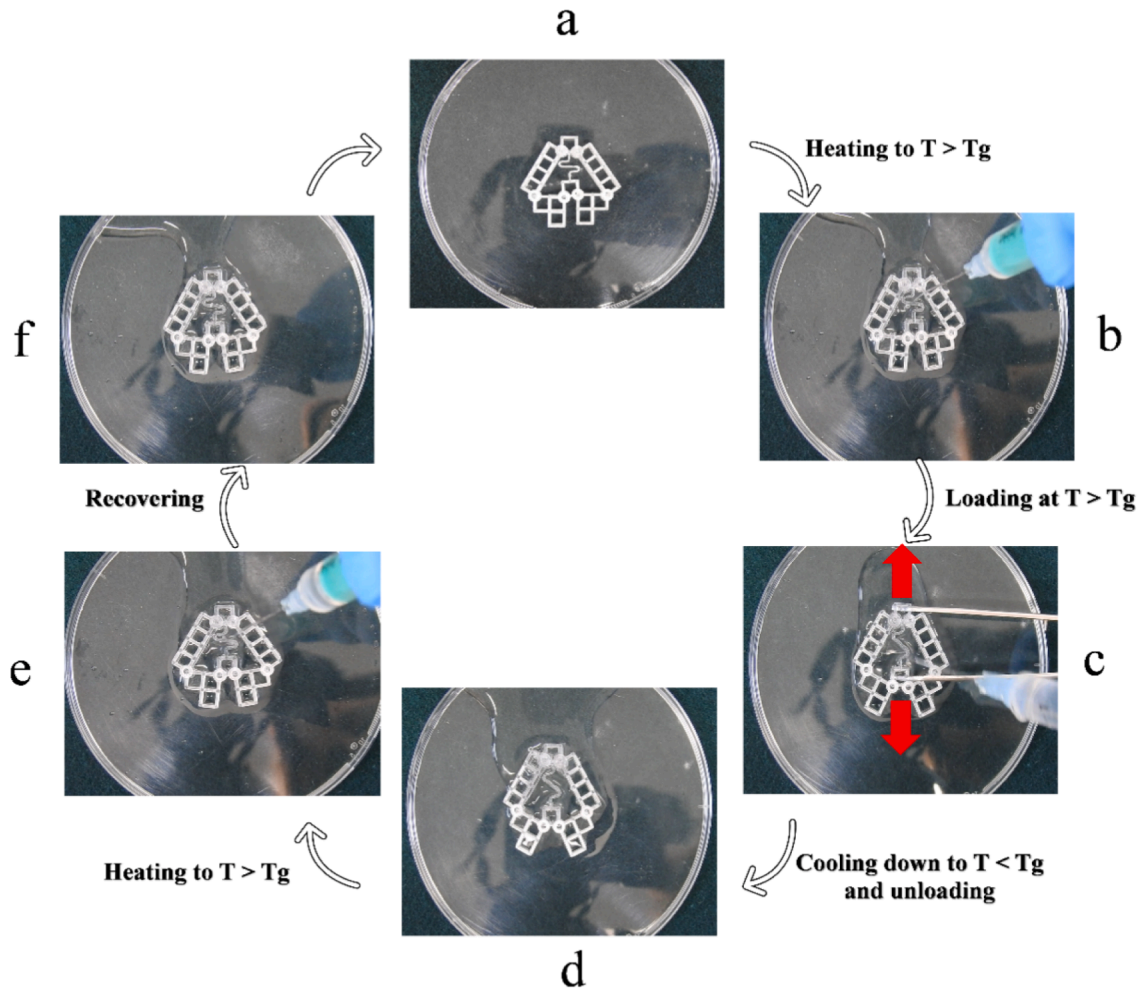


Fig. 7. The shape memory trial (thermomechanical cycle) conducted on a 3D-printed complex-shaped SMEp prototype. (a) The original state of the prototype. (b) Local heating of the actuator with hot water ($T_g + 20\text{ }^\circ\text{C} = 75\text{ }^\circ\text{C}$). (c) Deforming the heated actuator and local cooling of the deformed actuator with cold water ($T_g - 20\text{ }^\circ\text{C} = 25\text{ }^\circ\text{C}$) while keeping the deformation constant. (d) Obtaining the temporarily deformed prototype after removing the force from the actuator: shape fixity. (e) Local heating of the actuator with hot water ($T_g + 20\text{ }^\circ\text{C} = 75\text{ }^\circ\text{C}$). (f) Obtaining the original shape of the prototype: shape recovery.

reheating the actuator to $75\text{ }^\circ\text{C}$ ($T_g + 20\text{ }^\circ\text{C}$) under the no-load condition (Fig. 9c).

We determined the mean θ_0 , θ_m and θ_{ir} in the prototypes containing the S-shaped spring based on the left and right apex angles in each step of the trial. [Supplementary Material S2](#) includes the changes in the angle values in each device during the thermomechanical trial. The final results of shape recovery mean values for different deformation levels are shown in [Table 4](#). The high shape recovery values of the prototypes with S-shaped springs, and excellent shape recovery of the t-shaped prototype with a torsional spring despite 97% deformation, prove how the shape memory behaviour empowers the design structure of the prototypes, amplifies the shape-shifting ability of the 3D-printed complex-shaped prototypes, by being responsive to stimuli within their environment.

Due to the water-resistant properties (water absorption of 0.2–0.4% according to material's datasheet and D570-98), the chosen SMEp is an ideal material to design multipurpose devices activated by immersion in water or by local application of water. Therefore, for fixing and recovery of the deformed shape, in addition to local actuation, the prototypes can be immersed in cold and hot water, respectively. It is worth mentioning that all types of the 3D-printed prototypes recover almost 100% by immersion in water. [Supplementary Material S3](#) shows videos of their functionality in water. These findings ease the path for the design and

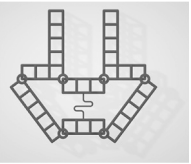
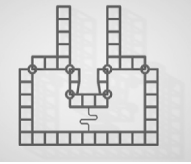
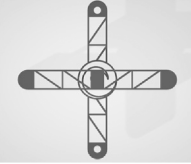
manufacture of adaptive products that can transform and respond to their environment, thereby enhancing their functionality and versatility. The successful integration of shape memory materials with 3D printing technology has the potential to transform several fields of engineering and pave the way for the development of cutting-edge products with unparalleled capabilities and performance.

3.4. Limitations of the study and future research proposals

The study of thermomechanical properties performed has focused on the thermal expansion and shape memory properties of the additively processable epoxy photorein and on design strategies for multiplying the shape-morphing through kinematic mechanisms and special joints. Our previous experiences with shape memory epoxies have made us focus on single actuation cycles without antagonistic forces, in connection with the design of one-step deployable structures. The study, and similar studies dealing with shape memory properties of polymers, especially pursuing high-performance actuators, may not only consider thermal expansion and shape memory properties, but could also take into account the effects of accumulated training and actuation processes and the effects of opposing loads on the shape recovery and fixity levels. To this end, following methods described in seminal studies in the field

Table 4

Mean values of shape deformation and shape recovery in the 3D-printed complex-shaped SMEp prototypes.

Prototypes	S_d (%)	S_{r0} (%)
1 	28.51	95.28
2 	34.16	92.83
3 	17.815	95.77
4 	97.175	93.46

is advised [31,32].

Mitigation strategies for minimizing the potentially negative effects of thermal expansion should be further explored. Part of the mitigation is already present in the described designs, in which the local distribution of actuators and the employment of kinematic chains help to avoid the thermal expansion of the whole structure, an only affects the S-shape actuating springs. Another effective approach to eliminate the influence of thermal expansion is by utilizing an SMP with a T_g close to room temperature. This characteristic enables cold drawing at lower temperatures, eliminating the need to heat the material above T_g to facilitate deformation. Incorporating specific nano-particles into an SMP presents another viable solution to mitigate the effects of thermal expansion. However, this approach also requires a thorough and systematic characterization of the shape memory polymer and eventual nano-particle systems in the case of shape-memory composites.

Furthermore, although thermal expansion is usually neglected or not fully considered in the design process, it could still be controlled or adjusted by the incorporation of special mechanical metamaterials to the designed geometries, as some studies have proposed based on origami principles [33].

In our view, apart from mitigating the effects of thermal expansion, perhaps it would be wise to take benefit from them. This could lead to multiple actuation steps, including: 1) precise and reversible thermal expansion and contraction-based actuations at temperatures below activation, and 2) larger shape transformations when heated beyond the activation temperature, for innovative micro/nanoelectromechanical systems (MEMS/NEMS), which constitutes an interesting future research direction.

It is worth mentioning that both thermoplastics and thermosets with remarkable shape memory properties have been studied and reported several times. In the case of thermoplastics, it is necessary to put forward their processability with fused-deposition modelling systems, probably the most widely available and accessible rapid prototyping systems based on 3D printing.

Indeed, the employment of 3D printers and thermoplastics has led to

a popularization of shape-memory actuators. At the same time, the possibility of additively processing elastomers using syringe-based printing and reaching compliant shape-morphing actuators driven by pressure is also outstanding [34]. Alternative interesting method is the use of multi-material printing of elastomers with different stiffness and expansion coefficients to reach reversible actuators capable of several actuation cycles [35]. Apart from the usual single-step actuation when employing shape-memory thermosets, like epoxy resins, another traditional drawback is that laser stereolithography systems are normally industrial machines and not very affordable. However, the recent progress with low-cost laser stereolithography systems and the possibility of processing thermosets with shape-memory properties employing cheap digital light processing systems are bound to make shape-memory thermosets more accessible.

An aspect that still renders thermosets unbeatable is linked to the surface quality, manufacturing precision and complex shapes achievable by additive photopolymerization systems, as compared with any other rapid prototyping and additive manufacturing approaches capable of processing smart materials. Certainly, processing of photoresins by micro-stereolithography or by two photon polymerization enables micrometric and submicrometric details to be achieved, which even enable 4D printing in the micro- and nanoscale for smart MEMS/NEMS applications [36–37].

In any case, authors foresee a future of multi-stimuli responsive actuators, in which different polymers, including polyurethane shape memory polymers [38–40] and those processed through a plethora of additive manufacturing technologies, are integrated into versatile devices capable of reversibly responding to temperature, pressure, electromagnetic fields and other environmental cues.

4. Conclusion

The thermomechanical properties of a multipurpose epoxy resin for laser stereolithography (SLA) have been explored, putting forward the relevance of considering both thermal expansion and shape-memory properties for the adequate design of shape-morphing actuators and devices. The complex shapes attainable with additive technologies and the precision achievable with additive photopolymerization enables the direct manufacture of mechanisms and the creation of functional gradients of thickness for defining compliant regions and localized actuators. Through these design strategies for additive manufacturing the shape-morphing performance of 3D or 4D printed actuators and devices can be promoted, as the study demonstrates.

To fulfil the objectives of the study, in the first part, we prepared dog-bone-shaped specimens, with the shape and dimensions selected during preliminary tests, made of epoxy resin by using SLA 3D printing. Our thermomechanical investigation of the SMEp revealed that according to the shape fixity and recovery values of the material (95% and 75%, respectively), the chosen material (SOMOS Watershed epoxy resin) possesses shape memory behaviour. However, significant thermal elongation of the polymer during thermomechanical testing had a negative influence on its shape recovery. We next produced high-resolution, high-quality 3D-printed prototypes, with innovative designs, made of epoxy resin also by SLA 3D printing. Each prototype contained an actuator, from which the device configuration could be changed. For fast actuation of the prototypes, instead of exposing the whole device to heat, we only subjected the actuator to activation, fixation and recovery by direct contact with hot and cold water, as the material is a thermally stimulated and water-resistant polymer. The localized actuators are connected to the rest of the structure through kinematic chains and compliant joints, which in addition multiply their action. The shape memory behaviour of the material makes it quite suitable for 4D printing of functional smart complex-shaped devices with precise configurational changes. Indeed, the SMEp shows a quick response to temperature and the deformed 3D-printed prototypes show excellent shape recovery.

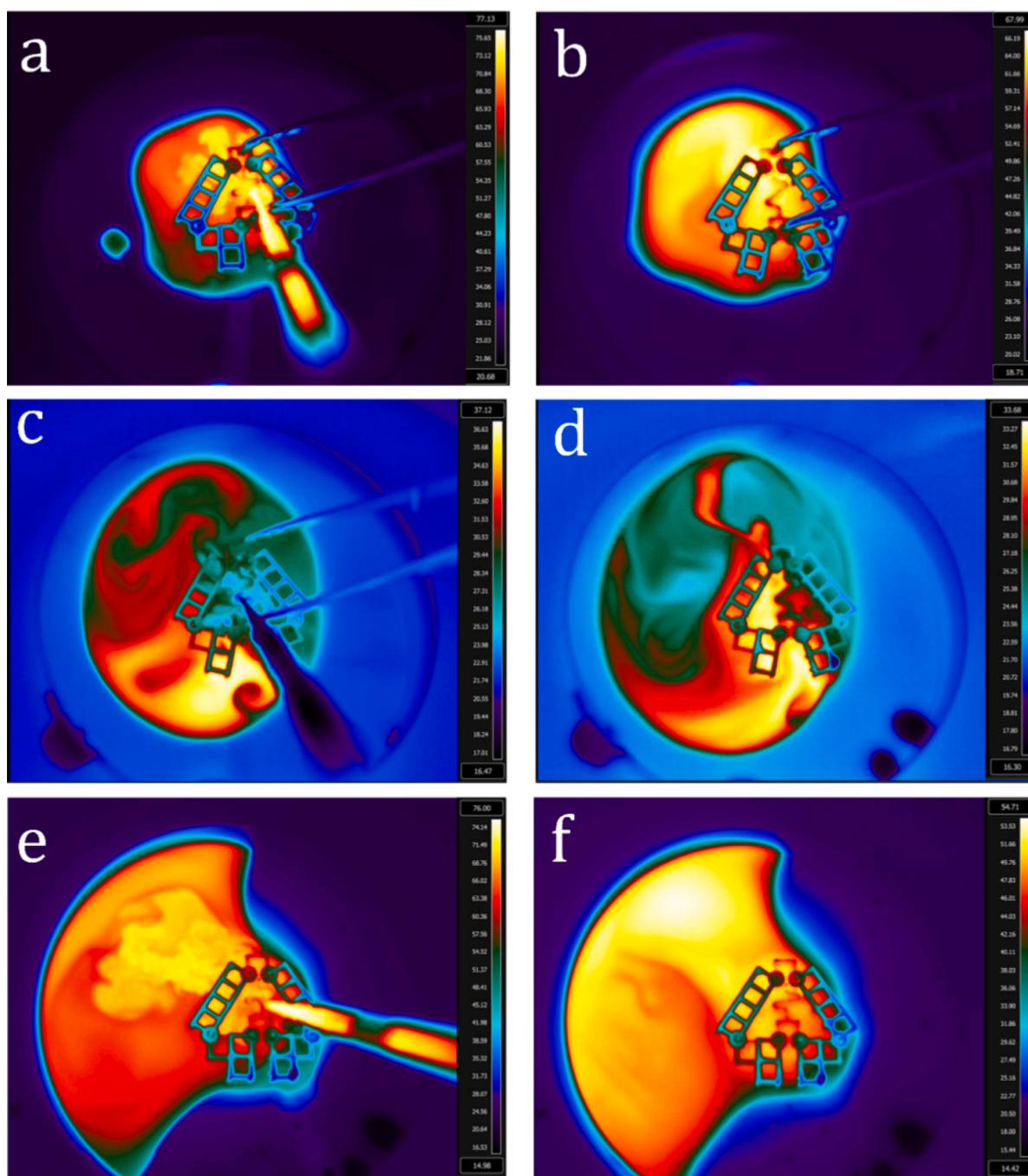


Fig. 8. The temperature profiles of a 3D-printed complex-shaped SMEp prototype during various stages of the thermomechanical cycle. (a) Local heating of the actuator with hot water ($T_g + 20\text{ }^\circ\text{C} = 75\text{ }^\circ\text{C}$). (b) Deforming the heated actuator. (c) Local cooling of the deformed actuator with cold water ($T_g - 20\text{ }^\circ\text{C} = 25\text{ }^\circ\text{C}$) while keeping the deformation constant. (d) Obtaining the temporarily deformed prototype after removing the force from the actuator: shape fixity. (e) Local heating of the actuator with hot water ($T_g + 20\text{ }^\circ\text{C} = 75\text{ }^\circ\text{C}$). (f) Recovery of the original shape of the SMEp prototype: shape recovery.

Multidisciplinary research, involving: (a) choosing and characterising a thermoresponsive shape memory polymer, (b) designing innovative devices to perform desired tasks, and (c) using a reliable manufacturing process to fabricate high-resolution, high-quality complex-shaped prototypes, led us to 4D printing of complex-shaped adaptive prototypes with prompt and precise shape-morphing properties.

In the future, multiple active regions could be incorporated within complex-shaped actuators and devices and the shape-morphing abilities of such active regions could be empowered through the use of kinematic chains, mechanisms and compliant joints. This approach would produce

more versatile actuators and lead to unconventional multi-stepped actuation in the area of shape-memory materials, as a complement to advances in triple shape memory polymers, and to extreme shape-morphing devices that may undergo several and quite radical geometrical transformations. Authors foresee applications in the development of smart medical devices and surgical tools, deployable structures for space and even exploratory robots for remote regions, which may be directly printed from the cloud at the point of service, without requiring any post-processing or assembly, as in the mechanisms, actuators and devices covered in this study.

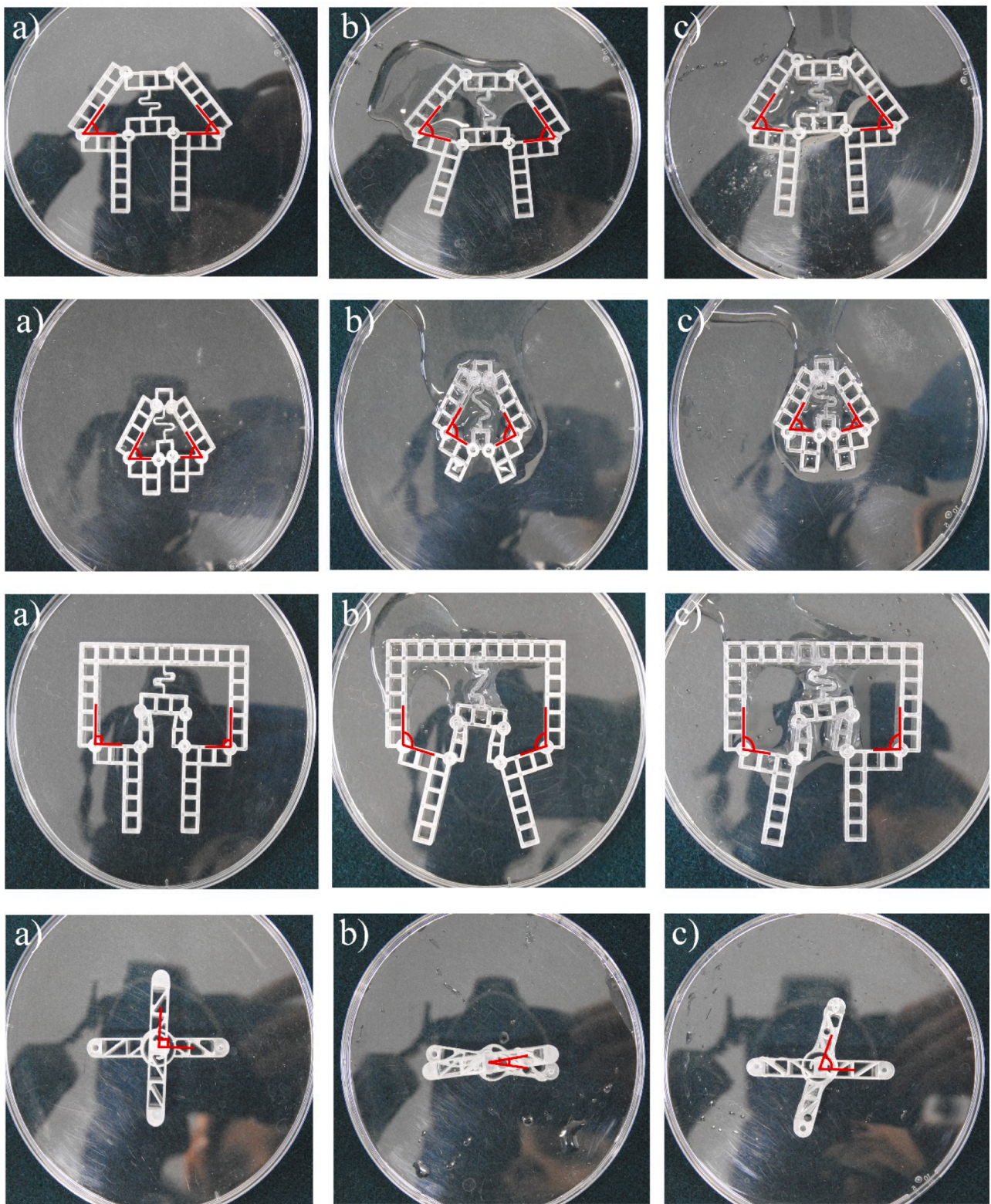


Fig. 9. (a) Original, (b) deformed and (c) recovered shape of the 3D-printed complex-shaped SMEp prototypes, programmed in a thermomechanical trial.

Declaration of Competing Interest

The authors declare that they have no known competing financial interests or personal relationships that could have appeared to influence the work reported in this paper.

Data availability

Data will be made available on request.

Acknowledgments

Authors are grateful for the support provided by the 14th call of the KMM-VIN research fellowship programme. This support enabled our collaborative research under the project titled “Investigation, Modeling, and Processing of Shape-Memory Polymers for Smart Micro-Actuators” between the Institute of Fundamental Technological Research Polish Academy of Sciences and Polytechnic University of Madrid. The call also supported a research stay of Mana Nabavian Kalat at UPM.

Authors would also like to acknowledge the National Science Centre in Poland, through grant 2017/27/B/ST8/03074, for supporting the research conducted at the IPPT PAN and the *Romanian Academy of Sciences* for funding the research conducted at the “*Petru Poni*” *Institute of Macromolecular Chemistry, Iasi, Romania*, under Polish - Romanian project for scientific cooperation titled “Interdisciplinary investigation of multifunctional polymeric materials”.

Elżbieta Pieczyska is also grateful to Hisaaki Tobushi, AICHI Institute of Technology and Shunichi Hayashi, SMP Technologies Inc. Japan, for introducing to SMP and much useful advices.

Andrés Díaz Lantada and Carlos Aguilar Vega acknowledge the support of research project “iMPLANTS-CM: impresión de metamateriales empleando aleaciones con memoria de forma y gradientes funcionales para una nueva generación de implantes inteligentes”, funded by the “Convocatoria 2020 de ayudas para la realización de proyectos sinérgicos de I + D en nuevas y emergentes áreas científicas en la frontera de la ciencia y de naturaleza interdisciplinaria” by Comunidad Autónoma de Madrid (ref.: Y2020/BIO-6756).

Authors acknowledge reviewers for their comprehensive comments and insightful proposals for improvement, which have helped us to reach a more objective, detailed and, hopefully, useful version of the manuscript.

Appendix A. Supplementary data

Supplementary data to this article can be found online at <https://doi.org/10.1016/j.matdes.2023.112263>.

References

- A.Y.N. Sofla, S.A. Meguid, K.T. Tan, W.K. Yeo, Shape morphing of aircraft wing: Status and challenges, *Mater. Des.* 31 (2010) 1284–1292, <https://doi.org/10.1016/j.matdes.2009.09.011>.
- S. Daynes, P.M. Weaver, Review of shape-morphing automobile structures: Concepts and outlook, *Proc. Inst. Mech. Eng. Part D J. Automob. Eng.* 227 (2013) 1603–1622, <https://doi.org/10.1177/0954407013496557>.
- H. Kim, S.-K. Ahn, D.M. Mackie, J. Kwon, S.H. Kim, C. Choi, Y.H. Moon, H.B. Lee, S. H. Ko, Shape morphing smart 3D actuator materials for micro soft robot, *Mater. Today* 41 (2020) 243–269.
- Q. Chen, P. Lv, J. Huang, T. Huang, H. Duan, Review Article Intelligent Shape-Morphing Micromachines, *Research* 2021 (2021).
- T.Y. Huang, M.S. Sakar, A. Mao, A.J. Petruska, F. Qiu, X.B. Chen, S. Kennedy, D. Mooney, B.J. Nelson, 3D Printed Microtransporters: Compound Micromachines for Spatiotemporally Controlled Delivery of Therapeutic Agents, *Adv. Mater.* 27 (2015) 6644–6650, <https://doi.org/10.1002/adma.201503095>.
- J.C. Kuo, H.W. Huang, S.W. Tung, Y.J. Yang, A hydrogel-based intravascular microgripper manipulated using magnetic fields, *Sens. Actuators, A* 211 (2014) 121–130, <https://doi.org/10.1016/j.sna.2014.02.028>.
- A. Díaz Lantada, A. De Blas Romero, E.C. Tanarro, Micro-vascular shape-memory polymer actuators with complex geometries obtained by laser stereolithography, *Smart Mater. Struct.* 25 (2016) 1–10, <https://doi.org/10.1088/0964-1726/25/6/065018>.
- M. Liu, L. Jin, S. Yang, Y. Wang, C.B. Murray, S. Yang, Shape Morphing Directed by Spatially Encoded, Dually Responsive Liquid Crystalline Elastomer Micro-Actuators, *Adv. Mater.* 35 (2023) 1–25, <https://doi.org/10.1002/adma.202208613>.
- T. Ashuri, A. Armani, R. Jalilzadeh Hamidi, T. Reasnor, S. Ahmadi, K. Iqbal, Biomedical soft robots: current status and perspective, *Biomed. Eng. Lett.* 10 (2020) 369–385, <https://doi.org/10.1007/s13534-020-00157-6>.
- R. Zapata Martínez, C. Aguilar, W. Solórzano-Requejo, O. Contreras-Almenger, C. Polvorinos Fernández, J. Molina-Aldareguia, A. Díaz Lantada, 4D Printed Surgical Devices: Current Capabilities and Challenges, *BIODEVICES 2023–16th Int. Conf. Biomed. Electron. Devices* 1 (2023) 157–163, <https://doi.org/10.5220/0011744300003414>.
- M.Y. Khalid, Z.U. Arif, R. Noroozi, A. Zolfagharian, M. Bodaghi, 4D printing of shape memory polymer composites: A review on fabrication techniques, applications, and future perspectives, *J. Manuf. Process.* 81 (2022) 759–797, <https://doi.org/10.1016/j.jmapro.2022.07.035>.
- X. Wan, Y. He, Y. Liu, J. Leng, 4D printing of multiple shape memory polymer and nanocomposites with biocompatible, programmable and selectively actuated properties, *Addit. Manuf.* 53 (2022), 102689, <https://doi.org/10.1016/j.addma.2022.102689>.
- J.W. Sohn, J.S. Ruth, D.G. Yuk, S.B. Choi, Application of Shape Memory Alloy Actuators to Vibration and Motion Control of Structural Systems: A Review, *Appl. Sci.* 13 (2023), <https://doi.org/10.3390/app13020995>.
- M. Staszczak, M. Nabavian Kalat, K.M. Golański, L. Urbański, K. Takeda, R. Matsui, E.A. Pieczyska, Characterization of Polyurethane Shape Memory Polymer and Determination of Shape Fixity and Shape Recovery in Subsequent Thermomechanical Cycles, *Polymers (Basel)* 14 (2022), <https://doi.org/10.3390/polym14214775>.
- Q. Zhao, H.J. Qi, T. Xie, Recent progress in shape memory polymer: New behavior, enabling materials, and mechanistic understanding, *Prog. Polym. Sci.* 49–50 (2015) 79–120, <https://doi.org/10.1016/j.progpolymsci.2015.04.001>.
- H. Tobushi, H. Hara, E. Yamada, S. Hayashi, Thermomechanical properties in a thin film of shape memory polymer of polyurethane series, *Smart Mater. Struct.* 5 (1996) 483–491, <https://doi.org/10.1088/0964-1726/5/4/012>.
- Y. Zhao, M. Hua, Y. Yan, S. Wu, Y. Alsaid, X. He, Stimuli-Responsive Polymers for Soft Robotics, *Annu. Rev. Control. Robot. Auton. Syst.* 5 (2022) 515–545, <https://doi.org/10.1146/annurev-control-042920-014327>.
- G. Ehrmann, A. Ehrmann, 3D printing of shape memory polymers, *J. Appl. Polym. Sci.* 138 (2021) 1–11, <https://doi.org/10.1002/app.50847>.
- P.L. Morgado, A.D. Lantada, H. Lorenzo-yustos, J. Muñoz-garcía, I.R. Martínez, A. J. Ramos, J. Luis, H. Riesco, Treatment of Mitral Valve Insufficiency By Shape Memory Polymer Based Active Annuloplasty, *Biodevices* 1 (2012) 17–22, <https://doi.org/10.5220/0001046400170022>.
- Q. Ji, M. Chen, X.V. Wang, L. Wang, L. Feng, Optimal shape morphing control of 4D printed shape memory polymer based on reinforcement learning, *Rob. Comput. Integr. Manuf.* 73 (2022), <https://doi.org/10.1016/j.rcim.2021.102209>.
- A.P. Piedade, 4D printing: The shape-morphing in additive manufacturing, *J. Funct. Biomater.* 10 (2019), <https://doi.org/10.3390/jfb10010009>.
- Y.J. Li, F.H. Zhang, Y.J. Liu, J.S. Leng, 4D printed shape memory polymers and their structures for biomedical applications, *Sci. China Technol. Sci.* 63 (2020) 545–560, <https://doi.org/10.1007/s11431-019-1494-0>.
- Y.Y.C. Choong, S. Maleksaeedi, H. Eng, J. Wei, P.C. Su, 4D printing of high performance shape memory polymer using stereolithography, *Mater. Des.* 126 (2017) 219–225, <https://doi.org/10.1016/j.matdes.2017.04.049>.
- H. Wu, P. Chen, C. Yan, C. Cai, Y. Shi, Four-dimensional printing of a novel acrylate-based shape memory polymer using digital light processing, *Mater. Des.* 171 (2019), 107704, <https://doi.org/10.1016/j.matdes.2019.107704>.
- C.A. Spiegel, M. Hippler, A. Münchinger, M. Bastmeyer, C. Barner-Kowollik, M. Wegener, E. Blasco, 4D Printing at the Microscale, *Adv. Funct. Mater.* 30 (2020) 1907615.
- A. Díaz Lantada, Systematic development strategy for smart devices based on shape-memory polymers, *Polymers (Basel)* 9 (2017), <https://doi.org/10.3390/polym9100496>.
- K. Shahi, R. Boomurugan, R. Velmurugan, Cold programming of epoxy-based shape memory polymer, *Structures* 29 (2021) 2082–2093, <https://doi.org/10.1016/j.istruc.2020.05.023>.
- K. Shahi, V. Ramachandran, Theoretical and Experimental Investigation of Shape Memory Polymers Programmed below Glass Transition Temperature, *Polymers (Basel)* 14 (13) (2022) 2753.
- I.S. Gunes, F. Cao, S.C. Jana, Effect of Thermal Expansion on Shape Memory Behavior of Polyurethane and Its Nanocomposites, *J Polym Sci B* 46 (2008) 1437–1449, <https://doi.org/10.1002/polb>.
- A. Lendlein, S. Kelch, Shape-Memory Polymers, *Angew. Chemie Int. Ed.* 41 (12) (2002) 2034–2057.
- Y. Liu, K. Gall, M.L. Dunn, P. McCluskey, Thermomechanics of Shape Memory Polymer Nanocomposites, *Mech. Mater.* 36 (10) (2004) 929–940.
- A. Lendlein, Shape Memory Polymers, in: *Advances in Polymer Science (Polymer)*, vol. 226, Springer, 2010, pp. 97–145.
- E. Boatti, N. Vasio, K. Bertoldi, Metamaterials: Origami Metamaterials for Tunable Thermal Expansion, *Adv. Mater.* 29 (26) (2017) 1700360.
- M. Mohammadi, A.Z. Kouzani, M. Bodaghi, Y. Xiang, A. Zolfagharian, 3D-Printed Phase-Change Artificial Muscles with Autonomous Vibration Control, *Adv. Mater. Technol.* 2300199 (2023).
- A. Zolfagharian, et al., Multimaterial 4D Printing with a Tunable Bending Model, *Smart Mater. Struct.* 32 (2023), 065001.

- [36] C.A. Spiegel, M. Hackner, V.P. Bothe, J.P. Spatz, E. Blasco, 4D Printing of Shape Memory Polymers: From Macro to Micro, *Adv. Funct. Mater.* 32 (2022) 2110580.
- [37] M. Islam, S. Hengsbach, D. Mager, J.G. Korvink, Nanoscale 3D Printing, *Encyclopedia of Materials: Electronics*. 1 (2023) 165–179.
- [38] E.A. Pieczyska, M. Maj, K. Kowalczyk-Gajewska, M. Staszczak, A. Gradyś, M. Majewski, M. Cristea, H. Tobushi, S. Hayashi, Thermomechanical properties of polyurethane shape memory polymer—experiment and modelling, *Smart Mater. Struct.* 24 (4) (2015) 045043.
- [39] Pieczyska E.A., , Maj M., Kowalczyk-Gajewska K., Golasiński K.M., Cristea M. , Tobushi H. , Hayashi S. , Investigation of thermomechanical couplings, strain localization and shape memory properties in a shape memory polymer subjected to loading at various strain rates, *Smart Mater Struct.*, 2016, 25, 8, 085002-1-15, doi: 10.1088/0964-1726/25/8/085002.
- [40] E. Pieczyska, M. Staszczak, K. Kowalczyk-Gajewska, M. Maj, K.M. Golasiński, S. Golba, H. Tobushi, S. Hayashi, Experimental and numerical investigation of yielding phenomena in shape memory polymer subjected to cyclic tension at various strain rates, *Polym. Test.* 6333–342 (2017), <https://doi.org/10.1016/j.polymertesting.2017.04.014>.